Understanding flow characteristics from tsunami deposits at Odaka, Joban coast, using a DNN inverse model

Rimali Mitra[1], Hajime Naruse[2], and Tomoya Abe[3]

[1]Connected Places Catapult. 1 Sekforde St. London, EC1R, 0BE, UK

[2]Division of Earth and Planetary Sciences, Graduate School of Science, Kyoto University, Kitashirakawa Oiwakecho, Kyoto, 606-8502, Japan

[3]Research Institute of Geology and Geoinformation, Geological Survey of Japan, National Institute of Advanced Industrial Science and Technology (AIST), AIST Central 7, 1-1-1 Higashi, Tsukuba 305-8567, Japan

Correspondence: Hajime Naruse (naruse@kueps.kyoto-u.ac.jp)

Abstract. The 2011 Tohoku-oki tsunami inundated the Joban coastal area in the Odaka region of Minamisoma City, up to 2,818 m from the shoreline. In this study, the flow characteristics of the tsunami were reconstructed from deposits using the DNN (deep neural network) inverse model, suggesting that the tsunami inundation occurred in the Froude-supercritical condition. The DNN inverse model ~~successfully reconstructed flow conditions, such as~~ effectively estimated the tsunami flow parameters in the Odaka region, including the maximum inundation distance, flow velocity, maximum flow depth, and ~~concentration in the Odaka region~~ sediment concentration. Despite having a few topographical ~~instabilities~~ anthropogenic undulations that caused the ~~flow~~ inundation height to fluctuate greatly, the reconstructed maximum flow depth and flow velocity were reasonable and close to the values reported in the field observations. The reconstructed data around the Odaka region were characterized by an extremely high velocity (12.1 m/s). This study suggests that the large fluctuation of flow depths at the Joban coast compared with the stable flow depths at the Sendai plain can be explained by the inundation in the supercritical flow condition.

1 Introduction

The 2011 Tohoku-oki tsunami of Mw 9.0 occurred on March 11, 2011, and it affected a large region of eastern Japan. With a significant number of fatalities and losses, this tsunami is considered ~~as~~ one of the largest in Japan (Sato et al., 2014).

It is becoming clear that tsunami inundation patterns vary significantly from place to place, even in areas adjacent to each other in the same tsunami event. Many studies of tsunami deposits have been conducted in and around the Sendai plain (Naruse et al., 2012; Abe et al., 2012). ~~Among them Naruse et al. (2012) estimated that the flow velocity of the 2011 Tohoku-oki tsunami on the Sendai plain ranged from 2.4 to 2.7 m/s, based on the critical velocity for the bedload motion of the largest grain-size class in the deposits.~~ Several field surveys, aerial video records, and satellite images were used to understand the flow conditions of the 2011 Tohoku-oki tsunami by reconstructing the inundated area and the size of the tsunami ~~(Hayashi and Koshimura, 2013; Tanigawa et al., 2014). The tsunami~~ (Hayashi and Koshimura, 2013). The inundation height at the transect (Naruse and Abe, 2017; Mitra et al., 2020) of Sendai plain was comparatively low (6.5 above T.P) (Naruse and Abe, 2017), possibly caused by the divergence of wave reflection owing to the concave bathymetry and wide continen-

tal shelf (Sato et al., 2014). The flow velocity of 1.9–6.9 m/s was reported on the Sendai plain using aerial video records (Hayashi and Koshimura, 2013). ~~Several numerical models of sediment transportaion have been proposed to investigate the~~

25 ~~offshore propagation and inundation at~~ Furthermore, in Rikuzentakata City, the flow velocity of the 2011 Tohoku-oki tsunami was estimated to be larger than 2.4–2.7 m/s, based on the flow reconstruction by Naruse et al. (2012). This reconstruction was achieved by considering the critical velocity required for bedload motion specifically related to the largest grain-size category found within the deposits.

Compared to other regions, Joban Coast is estimated to have experienced extremely high-velocity inundation (Sanuki et al., 2013; Sato et

30 , even though they are located adjacent to the Sendai plain ~~(Sugawara et al., 2012, 2014).~~

(Figure 1). The waves around the Odaka region ~~at Fukushima prefecture~~ destroyed or damaged nearly all seawalls because of large ~~tsunami~~ inundation height and co-seismic land-level subsidence (Sato et al., 2014). ~~The~~ Sanuki et al. (2013) estimated the inundation flow velocity ~~in Fukushima was estimated to be~~ from video images near the mouth of the Kido River in the Minamisoma region to be distinctively higher than that in the Sendai plain~~. Sanuki et al. (2013) estimated the flow velocity to~~

35 ~~be 10—15~~, which was 10–15 m/s in the river and coastal plain~~from video images~~. Sato et al. (2012a) and Sanuki et al. (2013) conducted a numerical simulation of tsunami inundation and also estimated high velocity flows in the area. Sato et al. (2014) estimated a ~~the~~ flow velocity higher than 11 m/s from the collapse of buildings. ~~Thus, extremely high velocity inundation flows were presumed in this region, but the precise measurements of tsunami inundation flows in the~~ When the overtopping flow was generated from the elevated seawall crown, it led to a substantial increase in velocity (exceeding 11 m/s based on the principles

40 of the Bernoulli theorem) as it encountered the formerly dry soil surface behind the seawall. This sudden surge in velocity was a direct consequence of the flow cascading over the seawall and impacting the ground. Therefore, it is conjectured that the coastal areas of ~~Fukushima area have not been well examined because of~~ the Fukushima region experienced supercritical, high-velocity inundation flows. However, due to the Fukushima Daiichi Nuclear Power Plant disaster (Mori et al., 2011; Mimura et al., 2011), the specific mode of tsunami inundation flows in that region has not been extensively investigated.

45 Within the Joban Coast, the Odaka area preserves a wide range of tsunami deposits, so this area is essential for studying the diversity of tsunami inundation flow characteristics and depositional effects of the high-velocity tsunami inundation flows. Recently, Iijima et al. (2021) performed a tsunami inundation simulation based on the fault model of Tohoku University (https://www.tsunami.irides.tohoku.ac.jp/hokusai3/J/events/tohoku_2011/model/dcrc_ver1.2.pdf), suggesting that the inundation flow in this area reached 8.2 m/s. In addition, they conducted a field study examining the influence of artificial structures on

50 depositional characteristics. However, the influence of the high-velocity inundation flow on the tsunami behavior, which may be a Froude supercritical flow, requires further investigation in this area. Although the tsunami propagation pattern from the fault model of Tohoku University can be assumed to be reasonable on the whole, local topographic conditions may have altered flow characteristics, so it is desirable to independently verify whether the characteristics of the inundated flow in each area are calculated before the depositional analysis. ~~However, post-tsunami surveys were conducted by several groups, such~~

55 ~~as the Tohoku Earthquake Tsunami Joint Survey Group (TETJSG,) and Sato et al. (2012b), which estimated tsunami heights from the water mark. There are few studies of tsunami deposits around Minamisoma, as the area was restricted until June, 2012 (Sato et al., 2014) because of nuclear radiation. Thus, the tsunami deposits have been well preserved, the restrictions~~

~~prevented anthropogenic disturbances. Therefore, it is important to survey the Minamisoma area to quantitatively reconstruct the tsunami characteristics using numerical and experimental models for future tsunami hazard mitigation and to construct preventive structural measures (Shuto, 2019).~~

Here, we conducted an inverse analysis of tsunami deposits distributed in the Odaka region of Minamisoma area, Fukushima ~~, using the newly proposed method by Mitra et al. (2020, 2021) to estimate flow conditions of~~ to estimate the tsunami inundation ~~flow conditions~~ in the area. The tsunami deposits in this area have been well preserved because the restrictions prevented anthropogenic disturbances. Several inverse and forward models have been proposed to reconstruct flow conditions (Jaffe et al., 2012; Li et al., 2012; Sugawara and Goto, 2012; Johnson et al., 2016; Yoshii et al., 2018). Recently Mitra et al. (2020, 2021) proposed a new 1D inverse model using the deep neural network (DNN) and predicted reasonable flow conditions of the 2011 Tohoku-oki tsunami and the 2004 Indian Ocean tsunami from measured grain-size distributions and thickness at different locations, such as the Sendai plain and Phra Thong island, Thailand. This inverse model utilizes a forward model that incorporates the non-uniform, unsteady transport of suspended sediments with turbulent mixing. The DNN model can effectively quantify the maximum inundation distance, flow velocity, maximum flow depth, and sediment concentration. The major advantages of this model are that the hydrodynamic and sediment transportation settings of this model are more realistic than other models and the uncertainty calculation of the predicted results can be estimated using a jackknife method. The results of the inverse analysis were verified by field observations. ~~Using this method~~ Utilizing this approach for the 2011 Tohoku-oki tsunami ~~at~~ deposit in the Sendai plain, ~~the reconstructed inundation length was 4, 045 m which is close to the original maximum inundation distance of approximately 4~~Mitra et al. (2020) reconstructed the inundation length, ~~020 m; the values of the~~ run-up flow velocity~~was 5.4 m/s, which was close to the spatial average of the measurements that ranged from 1.9 to 6.9 m/s; and the estimated the~~, and the maximum flow depth ~~was 4.1 m, which was also within the range of the~~ of the tsunami. Reconstructed flow conditions closely approximated the in-situ measured values from the Sendai plain~~(Mitra et al., 2020). For~~. The method was also applied to the 2004 Indian Ocean tsunami at Phra Thong ~~island in Thailand , the~~ Island in Thailand Mitra et al. (2021). The reconstructed inundation distance~~was 1, 700 m, whereas the original inundation distance was approximately 2,~~ ~~000 m, the flow velocityand maximum flow depth were 4.6 m/s and 4.8 m, respectively (Mitra et al., 2021)~~velocity, and flow depth fell in the range of the actual measurements.

In this study, despite the complex topography of the region, we successfully reconstructed the flow properties of the 2011 Tohoku-oki tsunami, and the results were corroborated by field observations. This provided a better understanding of tsunami inundation flow in Froude supercritical and subcritical conditions, which vary depending on the region and topographical settings. There are few studies that deal with the supercritical or subcritical conditions of tsunami inundation flows (Qi et al., 2014; Sakakiyama, 2014) quantitatively. This study focuses on the ability of the DNN model to estimate the flow conditions, such as flow velocity ~~, flow depthete.~~and depth, and how those parameters can be used to delineate the Froude number (Fr) to understand the type of prevailing flow, such as subcritical ($Fr < 1$) or supercritical ($Fr > 1$), during tsunami inflow at different regions. Hence, the DNN inverse analysis results could be used to construct appropriate preventive structural measures for tsunami and mitigation strategies around the Minamisoma area (Shuto, 2019).

2 Topographic Setting and Tsunami ~~Characterities~~ Characteristics in Study Area

This study used the samples from Odaka ~~district~~ region of Minamisoma City (Figure 1), which is located 25 km north of ~~Fukushima prefecture (Oota et al., 2017; Koff et al., 2012)~~ the Fukushima nuclear power plant (Koff et al., 2012). The tsunami flooded a wide area with the river, which caused major damage to the properties in the Odaka lowland (Koff et al., 2012). The topographical features of the area include the gentle slope of the coastal plain, beach ridges, marshes, lagoons and sea dikes (Sawai et al., 2012; Koff et al., 2012). A co-seismic subsidence of 0.5–0.8 m has been reported from a few places in the Odaka region (Sato et al., 2012b, 2014) and this event caused a reduction of the sea-wall heights. The shoreline along Minamisoma was convex with the presence of alternating coastal bluffs and plains (20 m) which were associated with terrace-like seafloors consisting of steeper ascending slopes near the coastline (Tsuruta et al., 2017).
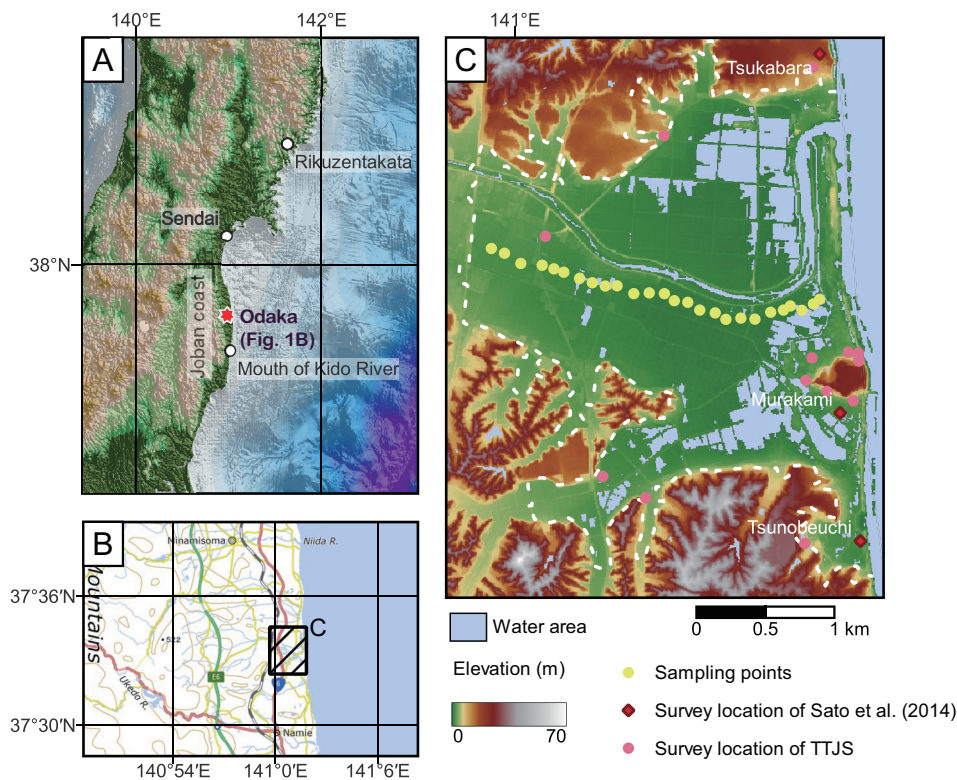
Figure 1. Location of the study area and sampling points. (~~A~~a), (~~B~~b) Location of study area. These maps are based on information from the Geospatial Information Authority of Japan and GEBCO 2023 Grid (https://doi.org/10.5285/f98b053b-0cbc-6c23-e053-6c86abc0af7b~~)~~). (~~C~~c) The sampling points of this study~~and (Sato et al., 2014)~~. Study sites of Tsunami Joint Survey Group (~~TETJSG~~TTJS) are also plotted. White dashed line indicates the inundation limit of 2011 Tohoku-oki tsunami (https://www.gsi.go.jp/kikaku/kikaku40014.html). This map is based on 5 m grid Digital Elevation Model published by Geospatial Information Authority of Japan in 2012.

Precise ~~tsunami flow~~ velocity measurement is absent in this area. The inundation heights were measured by Sato et al. (2014) and the ~~TETJSG~~ TTJS (The 2011 Tohoku Earthquake Tsunami Joint Survey) group (http://www.coastal.jp/tsunami2011/) at the Odaka region around the Joban coast. Large variations in inundation heights along the coastal line were observed within short distances in the region (Sato et al., 2014). This variation in inundation heights was caused by the complex coastal topography in Minamisoma City. ~~Figure~~ Figures 2a and b ~~shows~~ show the measured tsunami inundation heights ~~around the~~ as the distance from the shoreline increases along the Joban coast and the Sendai plain, and it is evident that the former shows a poor correlation with the ~~best fit~~ best-fit regression line, whereas the latter shows a strong correlation. The ~~data of inundation heights around the Odaka region were collected from the TETJSG () and Sato et al. (2014). The~~ topographic elevation for the ~~TETJSG data sets were~~ TTJS group data sets was calculated with a 5 m mesh DEM (~~GSI~~The Geospatial Information Authority of Japan) using several methods, such as adding surface information from a 3D ~~analyst tool, spatial analyst tool, etc. The elevations extracted from the DEM were confirmed using Google Earth and finally~~Analyst Tool and Spatial Analyst tool. Finally, the values were used to calculate a measured flow depth from the measured inundation height.
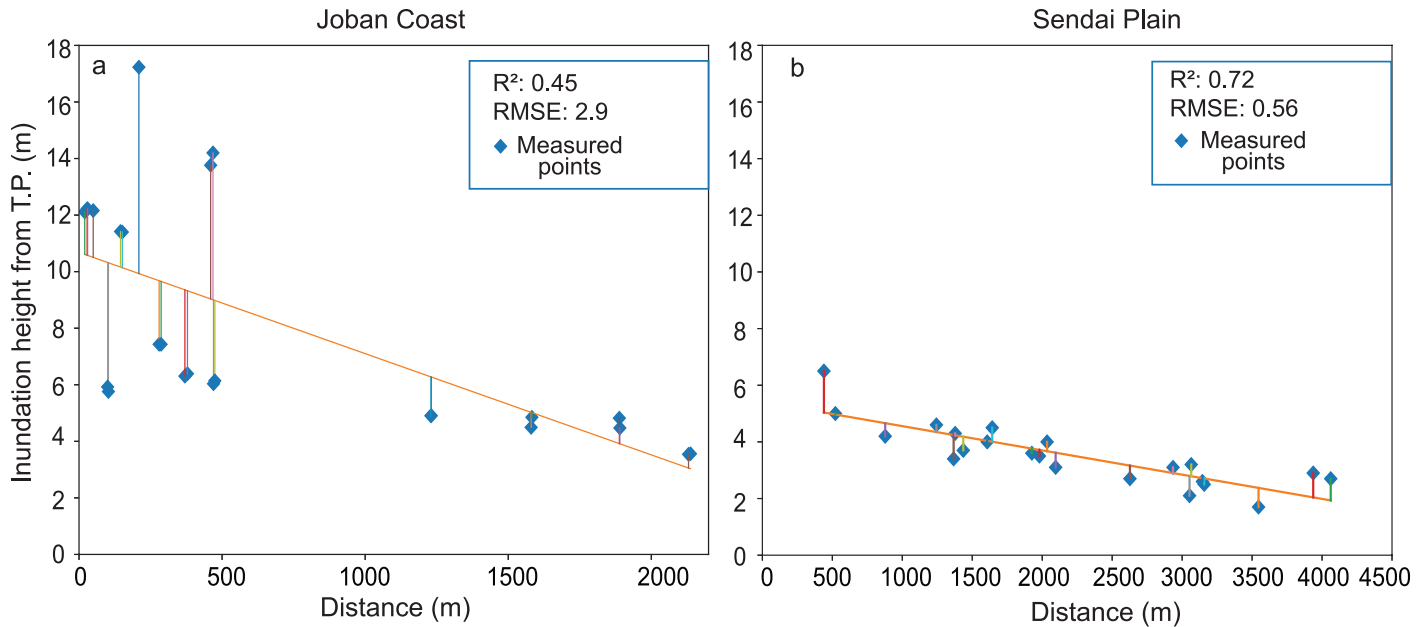
Figure 2. (a) Measured inundation heights of the 2011 Tohoku-oki tsunami around the Joban coast and Root mean square error (RMSE) and R^2 values show that the data points are away from the ~~best fit~~ best-fit line (b) Measured inundation heights at Sendai plain show that the measured flow depth of the 2011 Tohoku-oki tsunami around the ~~Joban coast~~ Sendai plain and Root mean square error (RMSE) and R^2 values show that the data points are close to the ~~best fit~~ best-fit line (Naruse and Abe, 2017). The data of inundation heights around the Odaka region were collected from the TTJS group and Sato et al. (2014).

In our study, the post-tsunami survey was conducted along the sampling transect ~~(Figure 1)~~(Figure 1c), perpendicular to the shoreline, and the samples were collected from 26 locations along the transect as shown in Figure 1. This survey was conducted

115 shortly after the site restriction was lifted (June 2012). The sampling was done every 100–200 m, and the thickness of the deposits was measured accordingly at each site. Grain-size analysis was performed using settling tubes with the Stube application program (Naruse, 2005). The procedures for the cleaning and pretreatment of samples followed the methods described in Naruse and Abe (2017).

3 Methodology

3.1 Forward model

120 The DNN inverse model incorporates the FITTNUSS forward model (Naruse and Abe, 2017), which is based on layer-averaged, 1D shallow water equations. This model calculates the spatial variation of the thickness and grain-size distribution of the tsunami deposits using the maximum inundation distance, flow velocity, maximum flow depth, and sediment concentration as the input values.

125 The fluid dynamics and sediment transport calculations encompass layer-averaged equations pertaining to the conservation of fluid mass, momentum, and sediment mass. The model operates under the quasi-steady flow assumption, positing that the velocity of tsunami run-up remains constant. At the same time, the inundation depth experiences a consistent increase until it attains its maximum value at the seaward boundary. Furthermore, it is postulated that the suspended sediment solely interacts with the bed sediment situated within the active layer on the surface of the bed, as proposed by Hirano (1971). The model necessitates the incorporation of several empirical closure equations related to fluid dynamics and sediment transport, including the entrainment rate of basal sediment, bed friction, and stratification of sediment concentration, as delineated by Naruse and Abe (2017).

The measured grain size distributions, spanning from 0 to 3 phi, were divided into six distinct grain size categories. To enable easier comparisons, these phi classes were converted into micrometers. In this study, the grain size distribution was discretized into six specific classes, each characterized by representative diameters of 841, 595, 420, 297, 210, and 149 μm. The corresponding phi scale values for these diameters are 0.25, 0.75, 1.25, 1.75, 2.25, and 2.75, respectively. The tsunami sedimentation was calculated using the Exner equation of bed sediment continuity of the ith grain-size classes, and the time variation of the grain-size distribution in the active layer was considered in the model (Hirano, 1971).

This model assumed that sediment entrainment and deposition occur during the run-up phase and that all the suspended sediment settled during the stagnant phase after the inundation. The coordinate transformation was applied for the efficiency and stability of the calculation of the fluid dynamics. The finite difference method was employed to obtain the numerical solutions in our model. The in-depth details of all the equations are provided in Naruse and Abe (2017) and Mitra et al. (2020).
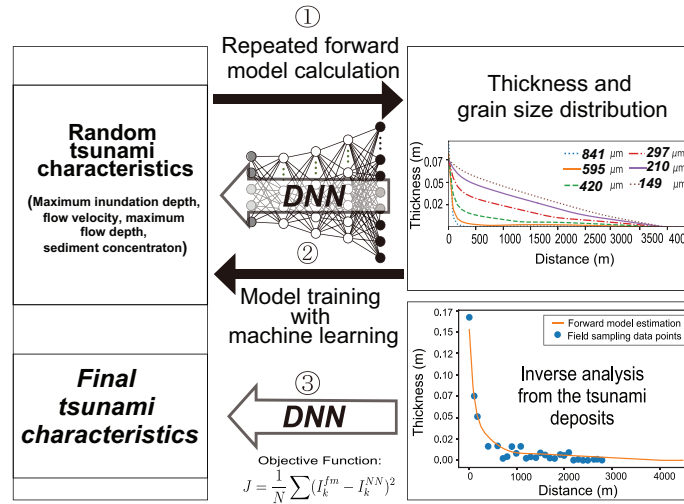
Figure 3. Workflow of DNN inverse model (modified from ~~Mitra et al., 2020~~Mitra et al. (2020)).

3.2 Inverse model

The DNN inverse model ~~consists of the~~ is composed of an artificial neural network ~~, with~~ featuring a total of five layers~~among them. There are~~, including three hidden layers. The input layer ~~accepts the values of~~ accommodates the values corresponding to the volume per unit area of ~~specific~~ grain-size classes at ~~specific~~ designated spatial grids. The ~~number of~~ volume values per unit area of sediment were calculated by multiplying the fraction of each grain size class in the grain size distribution by the deposit thickness. Here, the grain size distribution was obtained by averaging the measurements taken from samples at regular vertical intervals. The quantity of nodes and other hyperparameters ~~are the same as those used in Mitra et al. (2020) and Mitra et al. (2021). Finally, the output layer of the neural networkpredicts the~~ remain consistent with those employed in Mitra et al. (2020, 2021). Ultimately, the neural network's output layer generates predictions pertaining to flow conditions, such as maximum inundation distance, flow velocity, maximum flow depth, and sediment concentration.

Figure 3 shows the workflow of the DNN inverse model, which was trained using the artificial data set of depositional characteristics, such as thickness and grain-size distribution ~~which were~~ produced by random and repetitive ~~calculations of the forward model~~ forward model calculations. This was followed by ~~the validation of the~~ validating the performance using the artificial test data sets. A sampling window around the proximal part was used on the entire volume per unit area distribution to apply the inverse model~~as the~~. The distal part may contain large ~~error owing to~~ errors owing to the thinning of the deposits and field measurements potentially not covering the entire distribution of the deposits. The performance of the model was provided

in the supplementary information (Figure A1) as the performance results were almost similar to the results provided in Mitra et al. (2020) and Mitra et al. (2021).

After training and validation, the model was ready to apply to the field data set from Odaka region to reconstruct the flow condition of 2011 Tohoku-oki tsunami. For this investigation, we selected a sampling window size of 1,800 m, determined based on comparative results procured from tests employing varying sampling window sizes, as delineated in the results section. Within this study area, the grid spacing in fixed coordinates was set at 15 m, utilizing 120 spatial grids for the inversion process. Following the model's training, test data sets were subsampled at the sampling locations of the Odaka region (Figure 4 a–i). In this examination, sediment volume per unit area at the sampling locations was estimated via one-dimensional cubic interpolation. The subsampled data was subsequently re-interpolated at the forward model grids. The inversion was then applied to the subsampled data set. Consequently, the model's predictive accuracy was assessed by comparing the true values and the inversion results using the original test data sets to evaluate the bias induced by spatial distribution irregularities in the sampling locations.

3.3 Training and testing of the inverse model

The training and testing of the DNN inverse model has already provided evidence that the model has the promising ability to reconstruct tsunami flow characteristics. The final loss function values for the training and validation were 0.0039 and 0.0013, respectively, which were close to the previously reported values in Mitra et al. (2020) and Mitra et al. (2021). The sample standard deviation for the predicted and true values for the maximum inundation distance was small, 81.82 m, and it was only 0.26 m for flow velocity (Figure A1). There were no large deviations for any parameter. However, for the maximum flow depth, the model tended to estimate approximately 0.4 m lower than the original values on average, which is also very similar to 0.4 m and 0.5 m bias in Mitra et al. (2021) and Mitra et al. (2020) respectively. Correcting the final results by adding this bias to the model estimated values, the reconstructed results were compared with the field measurements. Before applying the model to the actual field data sets, the test data sets of the model were subsampled at the outcrop locations to investigate the bias that was caused by the effect of interpolation on irregularly spaced sampling locations. Consequently, the mean bias and sample standard deviation, attributable to irregular sampling spacing, were -16.9 m and 98.86 m for the maximum inundation distance, respectively. The bias and standard deviation for flow velocity were determined to be 0.2 m/s and 0.32 m/s, respectively. The maximum flow depth exhibited a mean negative bias of 0.5 m (Figure 4). Given that the parameter already possessed a bias of 0.4 m in the inversion outcomes of the original test data sets, the supplementary bias induced by the incompleteness of data sets amounted to
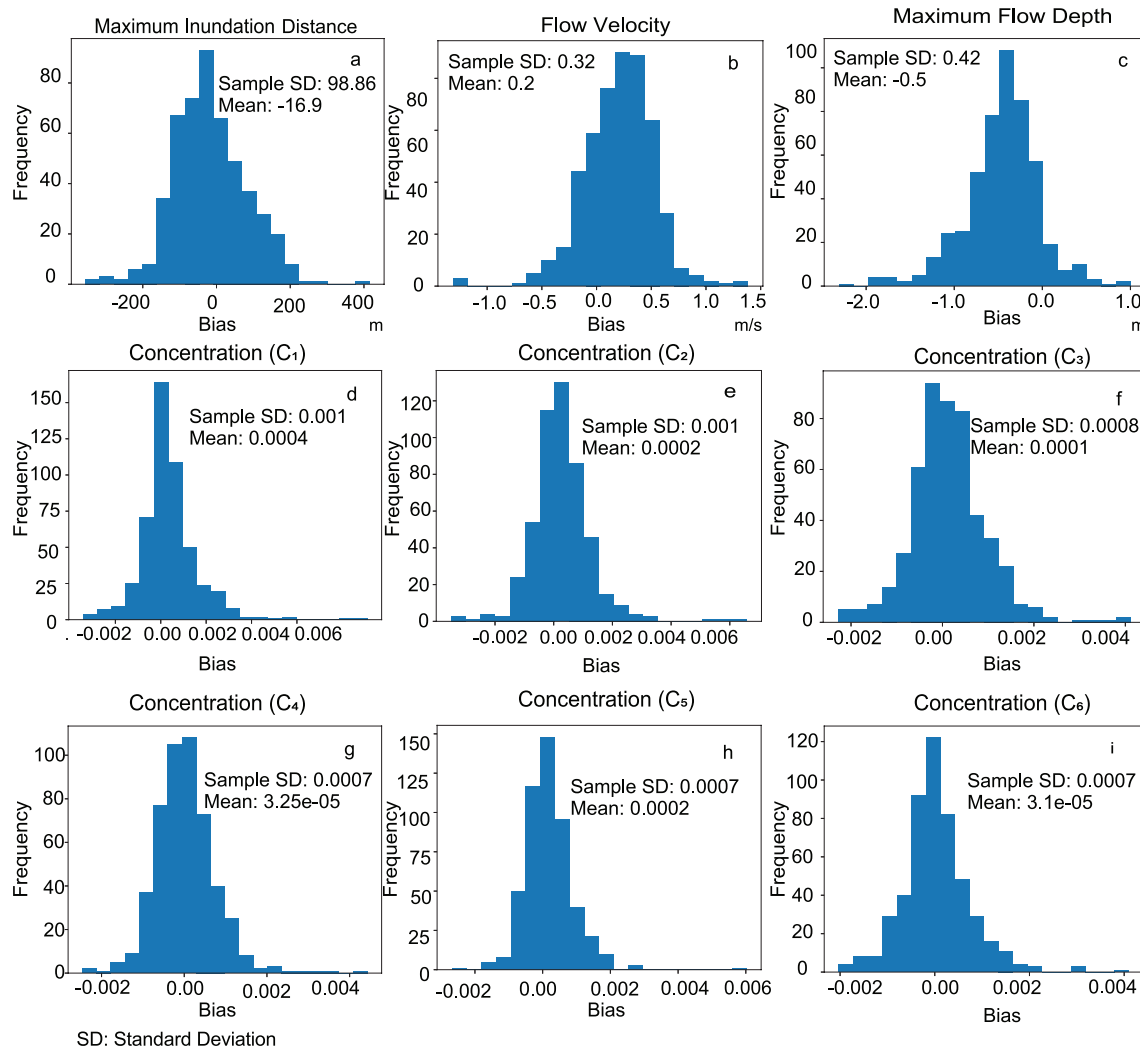
Figure 4. Histograms showing the variance and bias of predictions from the test data sets subsampled at the sampling locations of the transect at the Odaka region.

0.1 m~~toward negative end. Figures 4d–i show that the overall~~ . The mean bias in sediment concentrations was approximately ~~around~~ 0.01 % (Figures 4d–i).

The jackknife error variations were checked for different sampling window sizes. We chose a sampling window of 1,800 m for our study. Maximum inundation distance (Figure 5a), maximum flow depth, and concentration (Figure 5c, 5d, 5e) shows a decreasing trend with the sampling window size~~, but~~ . However, the flow velocity ~~shows~~ showed an increasing trend (Figure 5b). The change in the estimation error was very small after the sampling window size of 1,700 m.
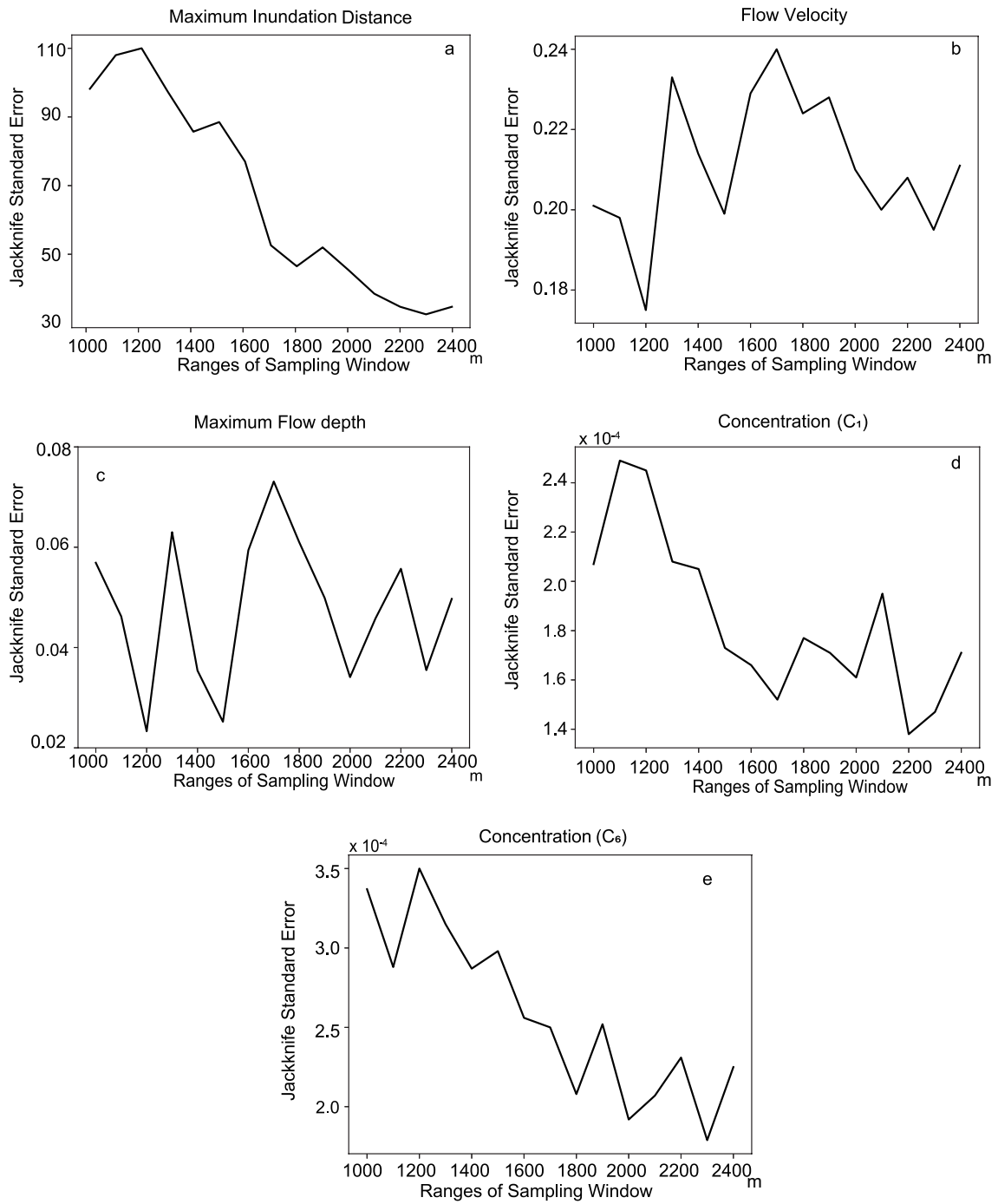
Figure 5. Changes of jackknife standard error with different sampling windows for different parameters.

4   Results

4.1   Grain-size and thickness of tsunami deposits

The maximum inundation distance in this study area was observed 2,818 m from the shoreline along the survey transect, and tsunami deposits were present from 183 to 2,563 m from the shoreline. The tsunami deposits consisted primarily of sand-sized
205   particles with an overlying mud layer. Mud layers ranged in thickness from 0.2 to 13.5 cm, and the ~~overall~~ sand thickness ranged from 0.5 to 22 cm. Sand layers were primarily composed of coarse to fine sand, with rip-up clasts and broken roots of vegetation. The spatial variation of grain-size distribution in the tsunami deposit was characterized by landward fining and thinning (Figure 6a). The tsunami deposits had a 22 to 6 cm ~~(Figure 6a)~~ thickness from the shoreline to around 1,600 m, whereas thinning of the deposits was observed after 1,600 m, ranging from 2 to 0.5 ~~m~~ cm to the maximum extent of the deposit
210   at the landward side (Figure 6a). The mean grain-size distribution from this region varies from 1.5 phi to 2.6 phi around the study area at Odaka (Figure 6b). Regarding sedimentary structures, the tsunami deposits in this area were characterized by a single layer of a fining upward sequence with parallel lamination showing a prominent color variation. The columnar sections and outcrop photographs are available in the supplementary materials (Figures S1 and S2).
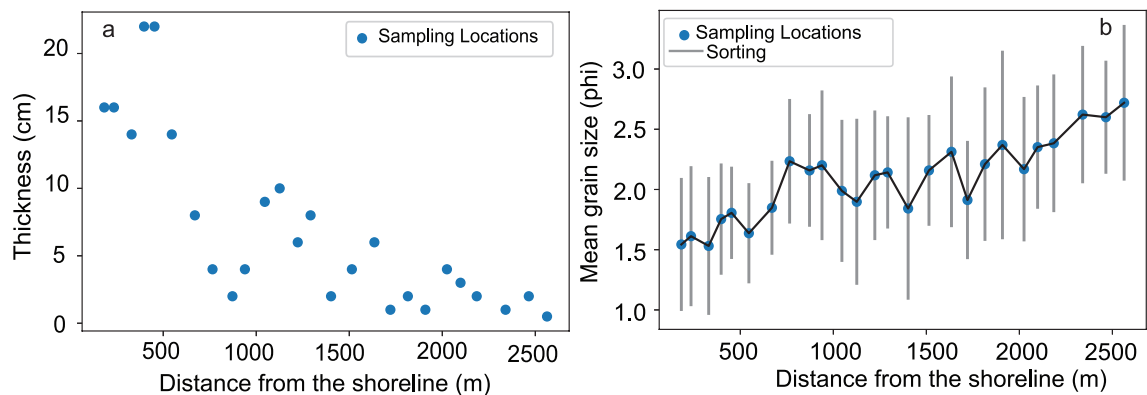
Figure 6. (a) Thickness of the deposits from the shoreline measured along the transect at Odaka. (b) Mean grain-size distribution and sorting of the deposits along the transect.

4.2   Inverse analysis of the 2011 Tohoku-oki tsunami deposits at Odaka

215   The maximum inundation distance at Odaka was reconstructed to be 2,897 m with a mean subsampling bias of -16.9 m (Table 1). The predicted flow velocity and maximum flow depth were 12.1 m/s and 2.4 m ~~respectively~~, respectively, with the mean subsampling bias of 0.2 m/s and -0.5 m. The total concentration of the sediment was 6.4% ~~with the concentration~~, with the concentrations of coarsest grain and finest grain-size classes were 0.5% and 2.1%, respectively (Table 1). Figure 7 shows the jackknife error estimates for different parameters ~~which were predicted by DNN model~~, which the DNN model predicted. For

 example, the 2σ estimation error of the maximum inundation distance was 91.1 m. The estimation error for the flow velocity was 0.4 m/s, and that for the maximum flow depth was 0.1 m (Figure 7a–c). The jackknife error estimates for sediment concentration were all very small, ranging around 0.02–~~0.05~~0.05% (Figure 7 ~~d-e~~d–e).

Using the reconstructed flow conditions of the tsunami by the DNN inverse model, the forward model was used to calculate the spatial distribution of the thickness and grain-size composition, and the measured distribution was compared with the

225 calculated distribution. Figure 8 shows the volume per unit area ~~,~~ and the grain-size distribution of measured and estimated values. The measured ~~values of volume~~ volume values per unit area for each grain-size class matched the predicted results for all grain-size classes.

5 Discussion

5.1 Verification of the tsunami characteristics reconstructed by the DNN inverse model with measurements

230 To verify our results, we compared the maximum flow depth reconstructed by the DNN inverse model with the measured values by ~~TETJSG~~ TTJS group and Sato et al. (2014) (Figure 9a and b). The locations measured by ~~TETJSG widely covers~~ the TTJS group widely covered the study area (Figure 2a). Sato et al. (2014) surveyed the surrounding areas around our field location~~,~~ ~~which are~~ : the Murakami, Tsunobeuchi, and Tsukabara~~areas~~. The Murakami and Tsunobechi areas are ~~situated~~ approximately 870 m, ~~and~~ 1,600 m south, respectively~~,~~ from the transect of this study, whereas Tsukabara is ~~situated~~ approximately 1,560 m

235 north from our field location. Sato et al. (2012b) measured the ~~tsunami~~ inundation height using mudlines ~~,~~ and damage marks on the artificial structures and trees. ~~TETJSG~~ TTJS group also measured the height using ~~water marks~~ watermarks soon after the event ~~took place~~ and before anthropogenic disturbances occurred from recovery. Figure 9a shows that the value of the predicted maximum flow depth approximated the average of the measured flow depth around Tsunobeuchi, Murakami, and Tsukabara, where the variability of the measured values was extremely large around the surveyed field locations of the study

240 area (Figure 2a). In contrast, the reconstructed maximum inundation distance was 2,897 ± 91.1 m, which was close to the observed extent of tsunami propagation that was around 2,818 m. Thus, although there was ~~a~~ large variability in the measured values of the inundation depth, the reconstructed results approximately reproduced the measured values~~approximately~~.

Regarding the flow velocity, the estimated velocity by the DNN inverse model was 12.1 m/s, which was higher ~~comparing~~ compared to the reconstruction in the Sendai plain (Mitra et al., 2020). The flow velocities of the 2011 Tohoku-oki tsunami

245 run-up flow were measured ~~at~~ 4.2 m/s on average, ranging from 1.9 m/s to 6.9 m/s from the aerial video records of the Sendai plain (Hayashi and Koshimura, 2013). In the 2004 Indian Ocean tsunami, flow velocities of ~~6-8~~6–8 m/s at the Khao Lak area, ~~3-4~~3–4 m/s~~added~~ at Kamala beach, 4 m/s at Phuket and 9 m/s at Khao Lak were observed (Rossetto et al., 2007; Karlsson et al., 2009; Szczuciński et al., 2012). The velocity measured from the survivors' videos of the December 26, 2004 Indian Ocean tsunami at Banda Aceh, Indonesia, was in the range of 2–5 m/s. (Fritz et al., 2006).

250 No direct observations of the flow velocity were made in this study area; however, the velocity was comparable with the values reported near the study area. Sanuki et al. (2013) used video footage analysis around the mouth of the Kido river, which is located 30 km ~~away from our field location~~ south of the field location of this study but along the ~~same~~ Joban coastline.
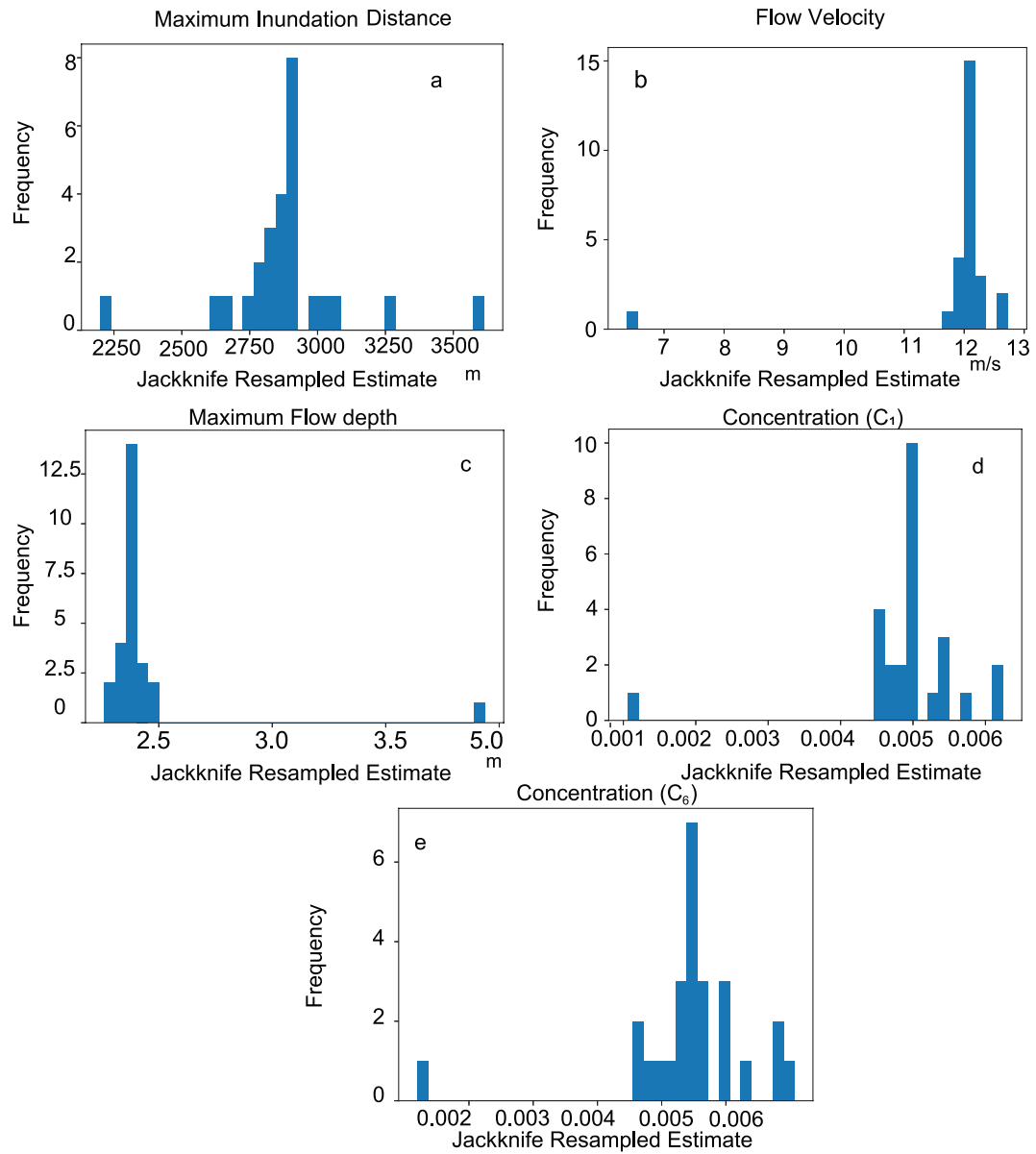
Figure 7. Jackknife resampled estimates for a sampling window size of 1,800 m for different parameters.
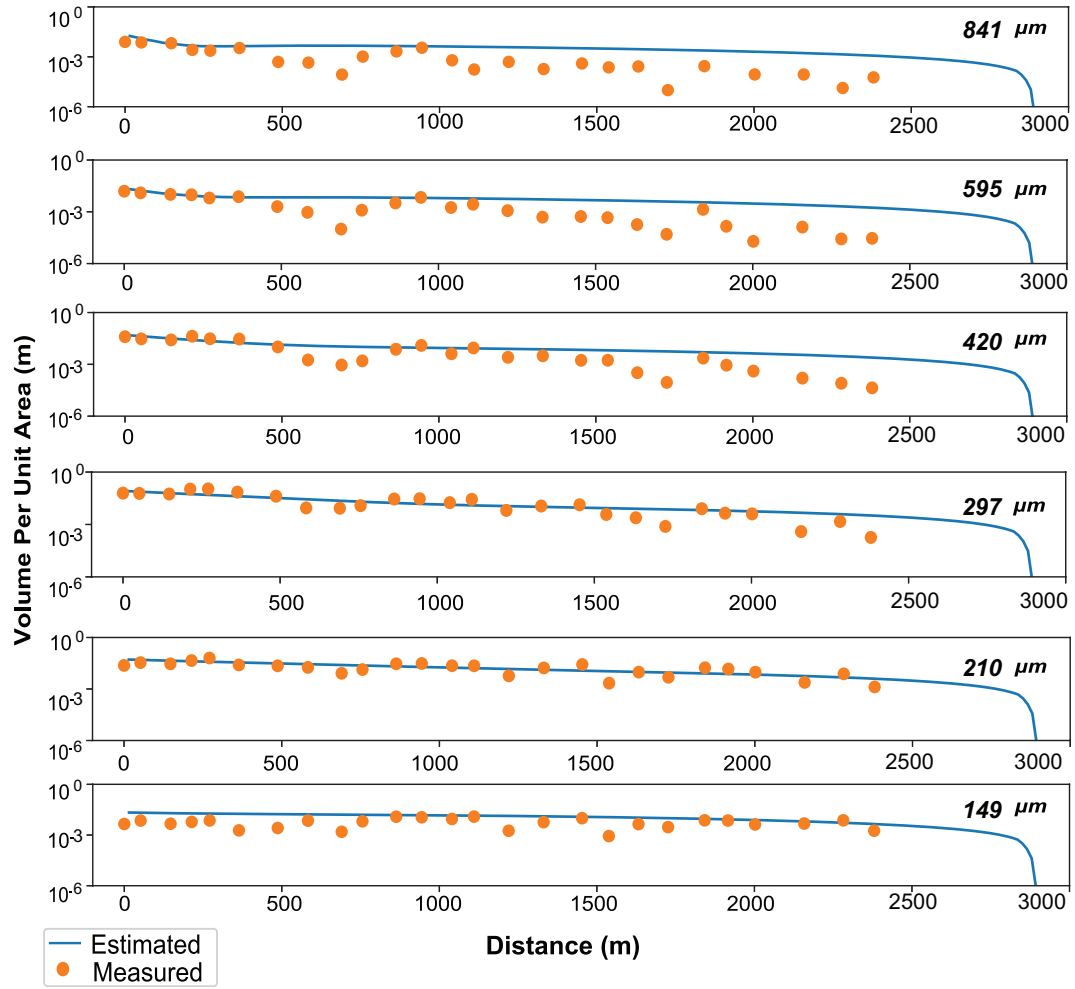
Figure 8. Spatial distribution of the volume per unit area of five grain-size classes. Solid circles indicate the values measured from the study area at Odaka, and lines indicate the results of the forward model calculation obtained using parameters predicted by the DNN inverse model.
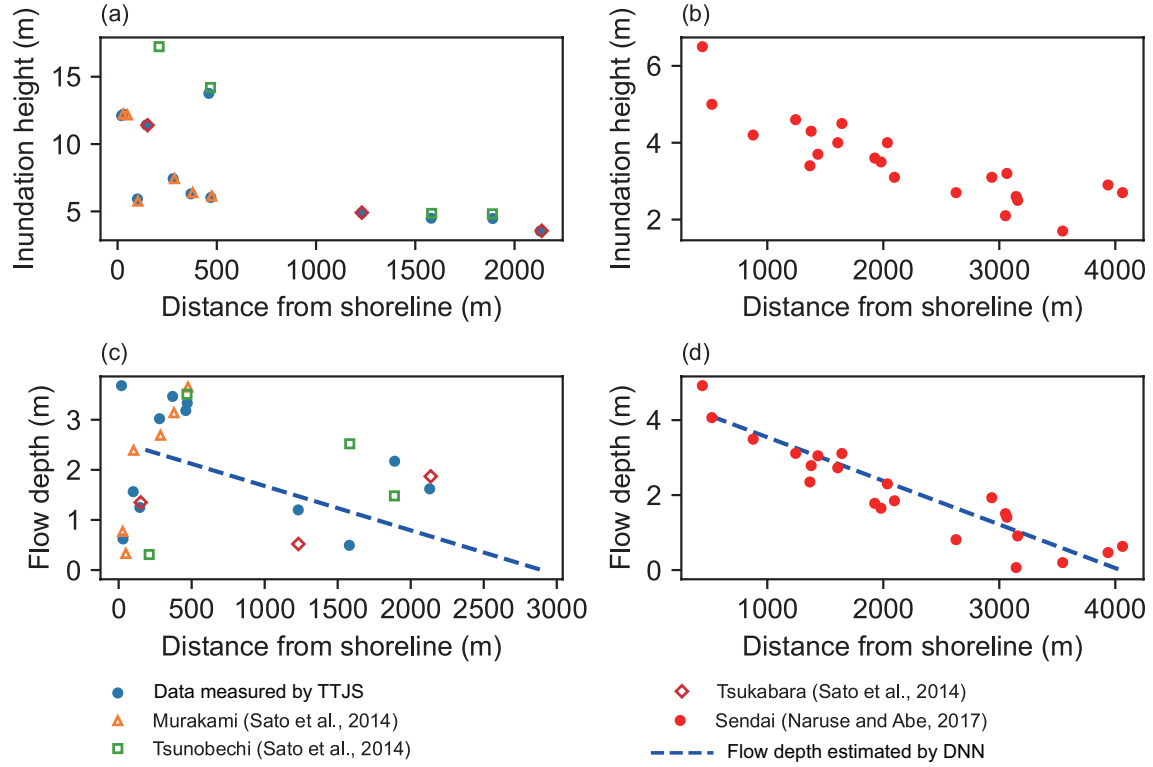
Figure 9. Measured maximum ~~inundation heights and~~ flow depths in Odaka and Sendai regions. Data were measured by ~~TETJSG~~ TTJS group (Mori et al., 2011), Sato et al. (2014) and Naruse and Abe (2017). (a) ~~Flow depths~~ Maximum inundation heights measured ~~at~~ in neighboring areas ~~are denoted by~~ of the ~~markers and~~ study sites (Figure 1C). (b) Maximum inundation heights measured in Sendai Plain (**??**). (c) The flow depth measured neighboring areas of the study sites (Figure 1C). The flow depth ~~estimated~~ reconstructed by ~~the~~ DNN ~~inverse model~~ is ~~shown~~ marked by the black dashed line. (~~b~~d) The flow depth measured ~~at the~~ in Sendai plain (Naruse and Abe, 2017). The flow depth reconstructed by DNN is marked by the ~~blue solid circle and the~~ black dashed line ~~shows the estimation by the DNN inverse model~~(Mitra et al., 2020).

They reported that the inundation flow was ~~14–11~~ 11–14 m/s inside the river channel, whereas it was around ~~15–10~~ 10–15 m/s in the coastal plain. Moreover, Sato et al. (2014) estimated that the overtopping flow on the seawall crown reached 11–17 m/s in velocity at the Idagawa area, which is located approximately 3 km south of the study area, based on the Bernoulli's theorem. Hence, the reconstruction of the flow velocity by the DNN inverse model is ~~said to be reasonable~~conformable in values measured in Joban Coast, suggesting that the exceptionally high flow velocity occurred in this area.

As a study of an area adjacent to this study area, our results are comparable with those estimated by Iijima et al. (2021). The forward model employed in this study approximates the behavior of tsunami inundation flows by two stages: the stage in which deposition occurs during the flooding current is flowing and the stage in which deposition occurs gradually after the flow has ceased (Naruse and Abe, 2017). The velocity of the actual tsunami inundation flow temporarily varies and is known to be very fast at the beginning but to decay rapidly. From past studies, the velocity in the first stage estimated in this study approximately reproduces the initial rapid inundation velocity of the actual tsunami inundation flow (Naruse and Abe, 2017; Mitra et al., 2020, 2021). Iijima et al. (2021) performed numerical simulations for an area approximately 1 km south of this study area and estimated that the inundation flow velocity in the coastal area (0.1 km from the levee) was 8.1 m/s in maximum. In addition, their calculations estimated a flow behavior in which the flooded flow rapidly decelerates inland (4.0 m/s) and then accelerates again to 8.3 m/s. Although these velocity values are relatively smaller than those estimated as the first-stage velocity in this study, their results also support our assumption that the flow in this area was faster than the tsunami inundation flow measured in the Sendai Plain. The large spatial variation in velocity in their reconstructions is probably due to the presence of artificial structures (roads) in the study area. While the flow slowed down significantly when overcoming the unevenness, the study area is a flat area with fields (1), so it is predicted that the inundation flow did not slow down and was inundated at high speed.

It should be noted, however, that their perspective on the research approach differs from that of this study because Iijima et al. (2021) performed tsunami inundation calculations using a forward model according to an existing fault model. Although they conducted a field survey of the sediments, they did not estimate the flow conditions from the sediments by inverse analysis. Even if the fault model is correct, tsunami inundation predictions by forward modeling are not always accurate due to local topography and model assumptions. This study provides new information on the behavior of tsunami inundation flows to the Joban Coast area from a new perspective of tsunami deposit inversion.

5.2 Influence of inundation by Froude supercritical flows

The reconstructed tsunami characteristics in the Odaka region using the DNN inverse model suggested that the type of inundation flow was a Froude supercritical condition. Here, the Froude number is defined as $Fr = U/\sqrt{gh}$, which represents the ratio of inertia to gravity forces. U denotes the layer-averaged flow velocity as defined above. The parameters g and h are the gravitational acceleration and flow depth, respectively. The DNN inverse model for the Joban coast suggested that the flow velocity U and the depth h are 12.1 m/s and 2.4 m, respectively, so that Fr is 2.5 (Table 1). This Fr value clearly indicates that the flow condition in the study area was the supercritical condition ($Fr = 2.5 > 1$). On the other hand, for the 2011 Tohoku-oki tsunami in the Sendai plain, the flow velocity and depth were 5.4 m/s and 4.1 m, respectively, in the reconstruction by Mitra et al. (2020), indicating that the flow type was subcritical ($Fr = 0.9 < 1$).

In general, $Fr < 1$ indicates subcritical flows ($Fr < 1$) that are relatively slow in velocity or thick in flow depth, and the water surfaces of the subcritical flows are flat and stable. The undulation of a subcritical flow surface exhibits an out-of-phase relationship with the shape of topography. In contrast, $Fr > 1$ indicates supercritical flows ($Fr > 1$), which behave as a rapid or thin and unstable flow (Charvet et al., 2017), with low flow resistance and high sediment transport (Phantuwongraj and Choowong, 2012). A higher flow velocity with a lower flow depth ~~are the main characteristics~~ is the main characteristic of a supercritical flow, and in some cases, supercritical flow can result in a hydraulic jump that causes the local dissipation of high flow energy (Muste and Hoitink, 2017; Retsinis and Papanicolaou, 2020). The water surfaces of supercritical flows exhibit an in-phase relationship with the topography, and the shape of the flow surface shows a large fluctuation that emphasizes the shape of the bottom surface. Therefore, if the tsunami inundated the area as a supercritical flow, the flow depth could be high locally because of topographic influences. ~~This may lead to a devastating situation for disaster prevention.~~

The inundation flows of ~~the~~ large-scale tsunamis, such as the 2004 Indian ~~ocean~~ Ocean tsunami, have been observed~~to~~, and other tsunamis show that the tsunami inundation flow can be subcritical or supercritical, with the range of the reported Froude number varying ~~ranged~~ from 0.7 to 2.0, depending on place (Matsutomi et al., 2005). Choowong et al. (2008) that deposits of the 2004 Indian Ocean tsunami indicate cross-lamination of anti-dunes as a supercritical flow condition, and this flow regime was dominant during the inflow. The occurrence of anti-dunes at the Andaman coast of Thailand suggested a supercritical flow condition at the depositional area, and the bed maintains an in-phase relationship with the free water surface (Simons et al., 1960; Middleton and Hampton, 1973; Kennedy, 1963). Thus, judging from the sedimentary structure, the supercritical flow condition was maintained in this area during the inundation of the tsunami. ~~Our inverse analysis revealed that such supercritical flow inundation of~~

Hayashi and Koshimura (2013) measured the velocity of the 2011 Tohoku-oki tsunami in the Sendai Plain from the video records and reported that the ~~large-scale tsunami also occurred in the Odaka region, whereas it did not occur in the Sendai area~~ 2011 Tohoku-oki tsunami was a supercritical flow in the area close to the coast. However, when they calculated the Froude number, the flow thickness was set to only 1 m or 2 m because they were interested in the behavior of the frontal part of the inundation flow. Nevertheless, the Froude number of the tsunami inundation flow exceeded unity in the Sendai plain only up to 1200 m from the shoreline. Considering that the central part of the flow reached a depth of 3–4 m, the Froude number is half of the value for the 1 m depth setting, indicating that the tsunami inundation flow was Fr-subcritical in most of the area in the Sendai Plain (Hayashi and Koshimura, 2013).

The difference in flow conditions between Odaka and Sendai is shown clearly in the measurements of inundation heights. Figure 2a indicates that the measured ~~flow heights fluctuating~~ inundation heights fluctuate largely along the transect at Odaka, compared with those at Sendai (Figure 2b). This difference can be interpreted as the result of supercritical flow conditions with topographical complexities in the Odaka region. Since the inundation flow was presumably subcritical in the Sendai plain, the water surface would have been stable even if there were local topographic changes. In the Odaka region, the water surface of the ~~inundaiton~~ inundation flow fluctuated largely in response to local topographic variations because of its Froude supercritical condition. The ~~the flow~~ inundation heights also varied to a great extent, such as in Idagawa, where they were exceptionally high (Sato et al., 2014).

Other possible reasons ~~of~~ for local fluctuations in flow depths could be the formation of hydraulic jumps, particularly in the Odaka region. The fluctuations in the tsunami inundation depths in the Odaka ~~district~~ region in the Minamisoma area could be due to the presence of a lagoon in that area, which caused the transition from a supercritical to a subcritical flow resulting in a
325 hydraulic jump (Matsutomi et al., 2001; Yamaguchi and Sekiguchi, 2015; Ali Hasan Muhammad and Tanaka, 2019).

The reason for the ~~large~~ significant differences in tsunami characteristics between Odaka and Sendai has not been determined yet, but several possibilities may explain it. First, it could be due to the offshore steeper bathymetry in the Odaka region than that in the Sendai plain (Tsuruta et al., 2017; Ikehara et al., 2014; Abe et al., 2012) and the convex-shaped shoreline, which possibly decreased tsunami energy dissipation (Sato et al., 2014). In contrast, the offshore bathymetry of the Sendai plain is gentle, and
330 the possible reason for the subcritical flow in the Sendai plain could be the presence of a coastal forest, which reduced the flow velocity significantly (Kusumoto et al., 2020). In some cases, the flow velocity becomes extremely high behind the coastal dikes near the shoreline, and the energy decreases gradually ~~owing to the presence of~~ due to different obstacles along the way (Sugawara, 2020). However, in the case of Odaka or the Joban ~~coast~~ Coast the supercritical flow has been observed in the depositional area, similar to the Andaman coast in Thailand (Choowong et al., 2008).

6   Conclusions

In this study, we reconstructed the flow conditions, such as the maximum inundation distance, flow velocity, maximum flow depth, and sediment concentration, of the 2011 Tohoku-oki tsunami, around the Odaka ~~district~~region, Minamisoma, at the Joban coast. Despite having a ~~gentle slope and~~ complex topography, the DNN inverse model successfully predicted the flow conditions of the tsunami. The maximum inundation distance was 2,897 $\pm$ 91.1 m~~which was~~, close to the observed extent of
340 2,818 m by field investigations. The flow velocity was 12.1$\pm$0.4 m/s, ~~which was~~ similar to the values reported from the video image analysis and numerical simulation results by different researchers. The maximum flow depth was 2.4$\pm$0.1 m, which also matched ~~with~~ the reported measured values of the maximum flow depth around the field study area. The flow condition along the transect was determined to be supercritical based on the results ~~by~~ of the DNN inverse model, and the reason behind that might be the topographical undulations or a hydraulic jump. The fact that different flow characteristics of the 2011 Tohoku-oki
345 tsunami varied depending on the location is the key feature of this study. ~~Further studies are needed to improve the present inverse model algorithm to remove the computational bias, and the forward model could be updated as a 2D model or be replaced by another forward model.~~ Thus, the DNN model involves a reasonable inverse analysis for different locations despite ~~of~~ having complex topography, and this model ~~has the potential to~~ can be used as a tool for tsunami hazard mitigation and disaster management.
350 Our study incorporates the flow-type characterization phenomenon along with the reconstruction of the tsunami flow conditions for the area. Especially ~~,~~ for the Odaka region, it showed high flow velocity with shallow flow depth, which is a typical phenomenon of a supercritical flow type. However, a detailed investigation of such a high flow velocity around the Joban coast ~~needs to~~ must be conducted in future studies, as supercritical flows with hydraulic ~~jump~~ jumps can cause extensive damage

Table 1. Predicted results from the inverse model when applied to the 2011 Tohoku-oki tsunami data obtained from Odaka, Joban coast. All reported standard error calculations were performed using a 95% confidence interval.

Parameters	Predicted Results	Mean Bias
Maximum inundation distance	2,897 m $\pm$ 91.1 m	-16.9 m
Flow velocity	12.1 m/s $\pm$ 0.4 m/s	0.2 m/s
Maximum flow depth	2.4 m $\pm$ 0.1 m	-0.5 m
Concentration of C_1 (841 μm)	0.5% $\pm$ 0.03%	0.04%
Concentration of C_2 (595 μm)	0.6% $\pm$ 0.02%	0.02%
Concentration of C_3 (420 μm)	1.3% $\pm$ 0.04%	0.01%
Concentration of C_4 (297 μm)	2.1% $\pm$ 0.04%	~~0..003~~0.003%
Concentration of C_5 (210 μm)	1.3% $\pm$ 0.05%	0.02%
Concentration of C_6 (149 μm)	0.6% $\pm$ 0.04%	0.003%

to the artificial structures and livelihoods. For future studies, there is a need for considerable research on the influence of
355 supercritical inundation flow of tsunamis in the coastal area.

Code and data availability. All codes, data, and supplementary figures used in this study were deposited in the repository Zenodo (https: //doi.org/10.5281/zenodo.4764153 and https://zenodo.org/doi/10.5281/zenodo.10027887)

Author contributions. RM: methodology, software, writing, and field observation. HN: conceptualization, methodology, software, writing, reviewing, and editing. TA: field survey, description of deposits, sampling, and grain size analysis.

360 *Competing interests.* All authors declare that: (i) no support, financial or otherwise, has been received from any organization that may have an interest in the submitted work; and (ii) there are no other relationships or activities that could appear to have influenced the submitted work.

Appendix A: Test of the inverse model using the artificial data sets

After training the model, using the test datasets, the deviation of the predicted values from the original values ~~were~~ was plotted on a histogram to check the model performance. There was no large bias except the maximum flow depth, which showed that the predicted values for this parameter were approximately 0.4 m lower than the input values.

365
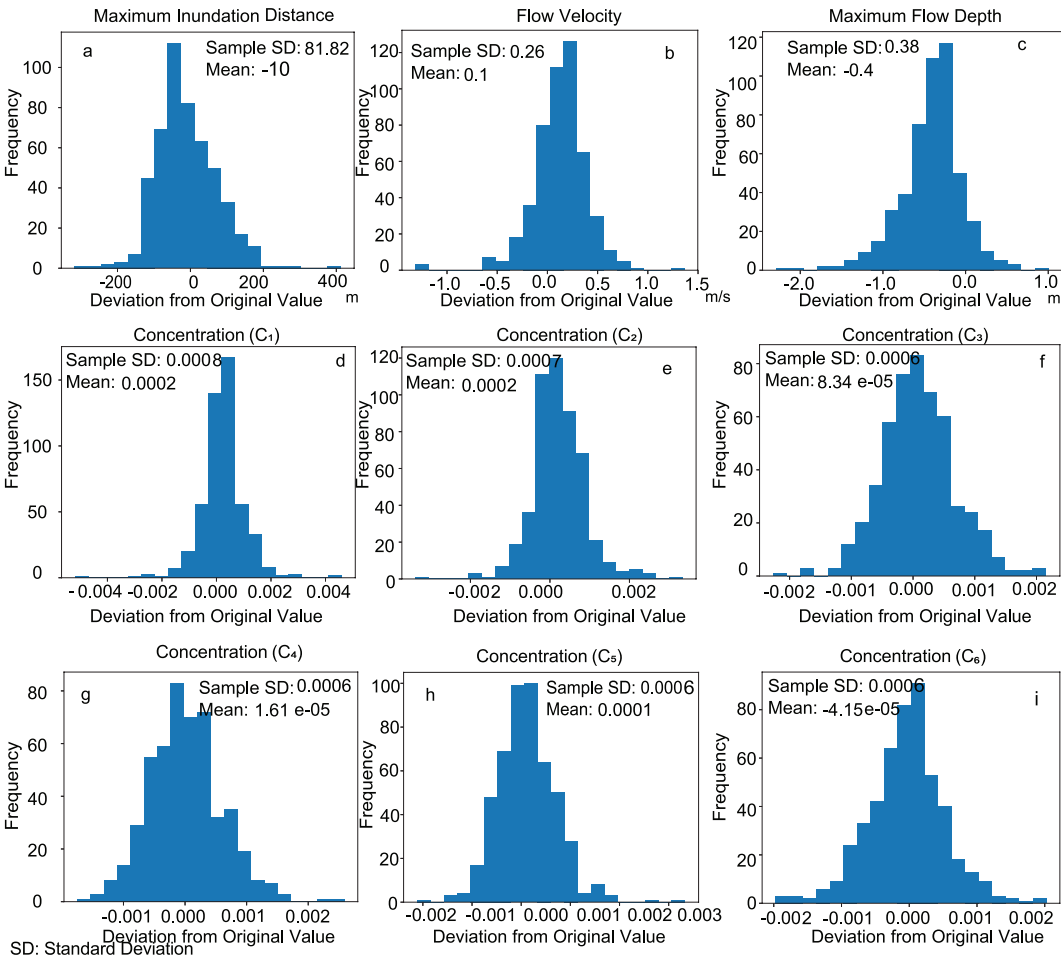
Figure A1. Histograms showing the deviation of the predicted results from the original values of the artificial test data sets.

Acknowledgements. We thank the Sediment Dynamics Research Consortium (sponsored by INPEX, JOGMEC, JX Nippon Oil and Gas Exploration Corporation, JAPEX), Advanced Industrial Science and Technology (AIST), Japan, for the funding ~~and~~. We also thank the Ministry of Education, Culture, Sports, Science and Technology, Japan, for providing the permission and scholarship for conducting this

370   collaborative research in Japan. We ~~also thank~~ acknowledge Dr. Kazuki Kikuchi, a post-doctoral fellow of Kyoto University, for performing

the grain-size analysis of the sediments from the tsunami deposits from the Odaka region.

References

Abe, T., Goto, K., and Sugawara, D.: Relationship between the maximum extent of tsunami sand and the inundation limit of the 2011 Tohoku-oki tsunami on the Sendai Plain, Japan, Sedimentary Geology, 282, 142–150, 2012.

375 Ali Hasan Muhammad, R. and Tanaka, N.: Energy reduction of a tsunami current through a hybrid defense system comprising a sea embankment followed by a coastal forest, Geosciences, 9, 247, 2019.

Charvet, I., Macabuag, J., and Rossetto, T.: Estimating tsunami-induced building damage through fragility functions: critical review and research needs, Frontiers in Built Environment, 3, 36, 2017.

Choowong, M., Murakoshi, N., Hisada, K. I., Charusiri, P., Charoentitirat, T., Chutakositkanon, V., Jankaew, K., Kanjanapayont, P., and
380 Phantuwongraj, S.: 2004 Indian Ocean tsunami inflow and outflow at Phuket, Thailand, Marine Geology, 248, 179–192, 2008.

Fritz, H. M., Borrero, J. C., Synolakis, C. E., and Yoo, J.: 2004 Indian Ocean tsunami flow velocity measurements from survivor videos, Geophysical Research Letters, 33, 2006.

Hayashi, S. and Koshimura, S.: The 2011 Tohoku tsunami flow velocity estimation by the aerial video analysis and numerical modeling, Journal of Disaster Research, 8, 561–572, 2013.

385 Hirano, M.: River bed degradation with armoring, Proceedings of Japan Society of Civil Engineers, 1971, 55–65, 1971.

Iijima, Y., Goto, K., Sugawara, D., and Abe, T.: Effect of artificial structures on the formation process of the 2011 Tohoku-oki tsunami deposits, Sedimentary Geology, 423, 105 978, 2021.

Ikehara, K., Irino, T., Usami, K., Jenkins, R., Omura, A., and Ashi, J.: Possible submarine tsunami deposits on the outer shelf of Sendai Bay, Japan resulting from the 2011 earthquake and tsunami off the Pacific coast of Tohoku, Marine Geology, 358, 120–127, 2014.

390 Jaffe, B. E., Goto, K., Sugawara, D., Richmond, B. M., Fujino, S., and Nishimura, Y.: Flow speed estimated by inverse modeling of sandy tsunami deposits: results from the 11 March 2011 tsunami on the coastal plain near the Sendai Airport, Honshu, Japan, Sedimentary Geology, 282, 90–109, 2012.

Johnson, J. P., Delbecq, K., Kim, W., and Mohrig, D.: Experimental tsunami deposits: Linking hydrodynamics to sediment entrainment, advection lengths and downstream fining, Geomorphology, 253, 478–490, 2016.

395 Karlsson, M, J., Skelton, A., Sanden, M., Ioualalen, M., Kaewbanjak, N., Pophet, N., Asavanant, J., and von Matern, A.: Reconstructions of the coastal impact of the 2004 Indian Ocean tsunami in the Khao Lak area, Thailand, Journal of Geophysical Research: Oceans, 114, 2009.

Kennedy, J. F.: The mechanics of dunes and antidunes in erodible-bed channels, Journal of Fluid Mechanics, 16, 521–544, 1963.

Koff, G., Borsukova, O., Popova, O., and Sidorin, A. Y.: On the causes of the great damage from the tsunami of March 11, 2011 on the
400 northeast coast of Honshu Island, Seismic Instruments, 48, 105–123, 2012.

Kusumoto, S., Imai, K., Gusman, A. R., and Satake, K.: Reduction effect of tsunami sediment transport by a coastal forest: Numerical simulation of the 2011 Tohoku tsunami on the Sendai Plain, Japan, Sedimentary Geology, 407, 105 740, 2020.

Li, L., Qiu, Q., and Huang, Z.: Numerical modeling of the morphological change in Lhok Nga, west Banda Aceh, during the 2004 Indian Ocean tsunami: understanding tsunami deposits using a forward modeling method, Natural hazards, 64, 1549–1574, 2012.

405 Matsutomi, H., Shuto, N., Imamura, F., and Takahashi, T.: Field survey of the 1996 Irian Jaya earthquake tsunami in Biak Island, Natural Hazards, 24, 199–212, 2001.

Matsutomi, H., Sakakiyama, T., Tsuji, Y., Tanioka, Y., Nishimura, Y., Kamataki, T., Murakami, Y., Matsuyama, M., and Kurizuka, K.: Challenges from the perspective of the 2004 Indian Ocean tsunami and damage estimates in and around Banda Aceh, Coastal Engineering Treatises, 52, 1366–1370, 2005.

410   Middleton, G. V. and Hampton, M. A.: Part I. Sediment gravity flows: mechanics of flow and deposition, Turbidites and Deep-Water Sedimentation, 1973.

Mimura, N., Yasuhara, K., Kawagoe, S., Yokoki, H., and Kazama, S.: Damage from the Great East Japan Earthquake and Tsunami-a quick report, Mitigation and adaptation strategies for global change, 16, 803–818, 2011.

Mitra, R., Naruse, H., and Abe, T.: Estimation of Tsunami Characteristics from Deposits: Inverse Modeling using a Deep-Learning Neural

415   Network, Journal of Geophysical Research: Earth Surface, 125, e2020JF005 583, https://doi.org/10.1029/2020JF005583, 2020.

Mitra, R., Naruse, H., and Fujino, S.: Reconstruction of flow conditions from 2004 Indian Ocean tsunami deposits at the Phra Thong island using a deep neural network inverse model, Natural Hazards and Earth System Sciences, 21, 1667–1683, https://doi.org/10.5194/nhess-21-1667-2021, 2021.

Mori, N., Takahashi, T., Yasuda, T., and Yanagisawa, H.: Survey of 2011 Tohoku earthquake tsunami inundation and run-up, Geophysical

420   Research Letters, 38, 2011.

Muste, M. and Hoitink, T.: Measuring flood discharge, in: Oxford research encyclopedia of natural hazard science, 2017.

Naruse, H.: Usage and advantages of an application program "STube" for settling tube grain-size analysis, Journal of the Sedimentological Society of Japan, 62, 55–61, 2005.

Naruse, H. and Abe, T.: Inverse Tsunami Flow Modeling Including Nonequilibrium Sediment Transport, With Application to Deposits From

425   the 2011 Tohoku-Oki Tsunami, Journal of Geophysical Research: Earth Surface, 122, 2159–2182, 2017.

Naruse, H., Arai, K., Matsumoto, D., Takahashi, H., Yamashita, S., Tanaka, G., and Murayama, M.: Sedimentary features observed in the tsunami deposits at Rikuzentakata City, Sedimentary Geology, 282, 199–215, 2012.

Oota, K., Ishizawa, T., and Hoyanagi, K.: Formation processes of tsunami deposits following the 2011 Tohoku-oki earthquake in the estuary of Odaka District, Minamisoma City, Fukushima Prefecture, Northeast Japan, Journal of the Sedimentological Society of Japan, 76, 3–16,

430   2017.

Phantuwongraj, S. and Choowong, M.: Tsunamis versus storm deposits from Thailand, Natural Hazards, 63, 31–50, 2012.

Qi, Z., Eames, I., and Johnson, E. R.: Force acting on a square cylinder fixed in a free-surface channel flow, Journal of Fluid Mechanics, 756, 716–727, 2014.

Retsinis, E. and Papanicolaou, P.: Numerical and Experimental Study of Classical Hydraulic Jump, Water, 12, 1766, 2020.

435   Rossetto, T., Peiris, N., Pomonis, A., Wilkinson, S., Del Re, D., Koo, R., and Gallocher, S.: The Indian Ocean tsunami of December 26, 2004: observations in Sri Lanka and Thailand, Natural Hazards, 42, 105–124, 2007.

Sakakiyama, T.: Tsunami pressure on structures due to tsunami inundation flow, Coastal Engineering Proceedings, pp. 42–42, 2014.

Sanuki, H., Takemori, R., Tajima, Y., and Sato, S.: Study on tsunami flooding in river based on video images and numerical simulation, in: Proceedings of Coastal Engineering, JSCE, vol. 69, pp. 196–200, 2013.

440   Sato, S., Liu, H., Takewaka, S., Nobuoka, H., and Aoki, S.-i.: Tsunami damages of Nakoso Coast due to the 2011 Tohoku Tsunami, Coastal Engineering Proceedings, pp. 2–2, 2012a.

Sato, S., Mizuhashi, K., Yeh, H., Isobe, M., Aizawa, H., and Ashino, H.: Coastal and nearshore behaviors of the 2011 Tohoku Tsunami along the central Fukushima Coast, Doboku Gakkai Ronbunshu B2. Kaigan Kogaku (Online), 68, 1–346, 2012b.

Sato, S., Okayasu, A., Yeh, H., Fritz, H. M., Tajima, Y., and Shimozono, T.: Delayed survey of the 2011 Tohoku Tsunami in the former
  exclusion zone in Minami-Soma, Fukushima Prefecture, Pure and Applied Geophysics, 171, 3229–3240, 2014.

Sawai, Y., Namegaya, Y., Okamura, Y., Satake, K., and Shishikura, M.: Challenges of anticipating the 2011 Tohoku earthquake and tsunami
  using coastal geology, Geophysical Research Letters, 39, 2012.

Shuto, N.: Tsunami hazard mitigation, Proceedings of the Japan Academy, Series B, 95, 151–164, 2019.

Simons, D. B., Rlchardson, E., and Nordin Jr, C.: Sedimentary structures generated by flow in alluvial channels, 1960.

Sugawara, D.: Chapter 4 - Trigger mechanisms and hydrodynamics of tsunamis, in: Geological Records of Tsunamis and Other Extreme
  Waves, edited by Engel, M., Pilarczyk, J., May, S. M., Brill, D., and Garrett, E., pp. 47–73, Elsevier, 2020.

Sugawara, D. and Goto, K.: Numerical modeling of the 2011 Tohoku-oki tsunami in the offshore and onshore of Sendai Plain, Japan,
  Sedimentary Geology, 282, 110–123, 2012.

Sugawara, D., Goto, K., Imamura, F., Matsumoto, H., and Minoura, K.: Assessing the magnitude of the 869 Jogan tsunami using sedimentary
  deposits: Prediction and consequence of the 2011 Tohoku-oki tsunami, Sedimentary Geology, 282, 14–26, 2012.

Sugawara, D., Goto, K., and Jaffe, B. E.: Numerical models of tsunami sediment transport—current understanding and future directions,
  Marine Geology, 352, 295–320, 2014.

Szczuciński, W., Rachlewicz, G., Chaimanee, N., Saisuttichai, D., Tepsuwan, T., and Lorenc, S.: 26 December 2004 tsunami deposits left in
  areas of various tsunami run up in coastal zone of Thailand, Earth, Planets and Space, 64, 5, 2012.

Tanigawa, K., Sawai, Y., Shishikura, M., Namegaya, Y., and Matsumoto, D.: Geological evidence for an unusually large tsunami on the
  Pacific coast of Aomori, northern Japan, Journal of Quaternary Science, 29, 200–208, 2014.

Tsuruta, T., Harada, H., Misonou, T., Matsuoka, T., and Hodotsuka, Y.: Horizontal and vertical distributions of 137 Cs in seabed sediments
  around the river mouth near Fukushima Daiichi Nuclear Power Plant, Journal of Oceanography, 73, 547–558, 2017.

Yamaguchi, N. and Sekiguchi, T.: Effects of tsunami magnitude and terrestrial topography on sedimentary processes and distribution of
  tsunami deposits in flume experiments, Sedimentary Geology, 328, 115–121, 2015.

Yoshii, T., Tanaka, S., and Matsuyama, M.: Tsunami inundation, sediment transport, and deposition process of tsunami deposits on coastal
  lowland inferred from the Tsunami Sand Transport Laboratory Experiment (TSTLE), Marine Geology, 400, 107–118, 2018.